**Center for Astrophysics**

Harvard College Observatory
Smithsonian Astrophysical Observatory

## MEMORANDUM

December 2, 1997

**To:** Steve Murray

**From:** Ralph Kraft

**Subject:** Shadowgraph and transmission measurements of backup HRC-I UVIS

**cc:** Martin Zombeck, Almus Kenter, Gary Meehan, Mike Juda

We have recently made x-ray shadowgraphs and transmission measurements on the backup HRC-I UV/Ion shield (filter is marked HRC-1007 Rev C S/N 009). The results of these measurements are summarized in this memo. All measurements were made in pipe #1 of the HRC laboratory. The model 5 Manson source (and source filters for the shadowgraphs), mounted at one end of the pipe, was used to create characteristic X-rays from several different anodes. A microchannel plate (MCP) detector with uncoated MCPs was attached to the other end of the pipe. The UVIS was mounted to two orthogonal translation stages which could be used to align the shield in both axes perpendicular to the beam, and to insert/remove the UVIS from the beam. A transmission grating (an LETG facet) and a slit were mounted on a vacuum feedthrough to disperse the incident spectra for the x-ray transmission measurements. The side arm proportional counter (monitor detector - MD) was used to monitor the temporal stability of the beam.

| Line | C $K_\alpha$ | O $K_\alpha$ |
|---|---|---|
| Anode | Graphite | $Mg(OH)_2$ |
| Filter | 33 $\mu$m poly | 2 $\mu$m Cr |
| Energy | 277 eV | 525 eV |
| IN filename | P1971007a.rd | P1971007d.rd |
| Integration time | 7200 s | 12400 s |
| MD rate | 222.434 cts/s | 378.369 cts/s |
| OUT filename | P1971007b.rd | P1971007c.rd |
| Integration time | 7200 s | 7200 s |
| MD rate | 97.573 cts/s | 375.685 cts/s |

Table 1: Summary of setup parameters for UVIS shadowgraph measurements.

# 1 Shadowgraphs

Shadowgraphs of the UVIS were made at two energies (C $K_\alpha$ and O $K_\alpha$) to measure the large scale uniformity of the shield. At each energy, two flat fields were taken, one with the shield in the beam (the IN image) and one with it withdrawn (the OUT image). The ratio of the two images (RATIO image=IN/OUT) then reflects large scale non-uniformity in the shield. Any spatial variation in the beam or detector divides out. Detector background was negligible for these measurements, and was not considered in the analysis. A summary of relevant test parameters is given in Table 1. The integration time was chosen to accumulate approximately 1000 cts/mm$^2$ in each image. The raw data were converted to images with the standard processing software, and was binned by a factor of 128 in both axes (pixels are 823 $\mu$m on a side).

These data were analyzed using two different techniques. In the first method, the distribution of the pixel values in the IN, OUT, and RATIO images at each energy was considered. The mean and variance of the distribution of pixel values for each of images was computed. These results are summarized in Tables 2 and 3 for the C $K_\alpha$ and O $K_\alpha$ measurements respectively. In all cases, the standard deviation of the IN and OUT distributions is consid-

| | Mean (counts) | Variance | Std Dev | $\sqrt{Mean}$ |
|---|---|---|---|---|
| IN image | 763.13 cts | 2537.25 | 50.37 cts | 27.62 cts |
| OUT image | 768.60 cts | 2516.28 | 50.16 cts | 27.72 cts |
| Ratio of means ($\mathrm{Mean}_{IN}/\mathrm{Mean}_{OUT}$) | | | | 0.993 |
| Statistical std dev of ratio | | | | **0.051** |
| Gaussian mean of RATIO image | | | | 0.988 |
| Gaussian sigma of RATIO image | | | | **0.050** |
| Transmission at C $K_\alpha$ | | | | **0.433** |

Table 2: Transmission of UVIS S/N 009 at C $K_\alpha$.

erably larger than the square root of the mean value of these distributions, indicating the presence of some type of spatial non-uniformity. The ratio and standard deviation (assuming counting statistics alone) of these means is also given. For comparison, a Gaussian was fit to the distribution of pixel values in each RATIO image. Plots of the distribution of pixel values in the RATIO images and the best fit Gaussians are contained in Figures 1 and 2. As can be seen from Tables 2 and 3, the centroid and width of these fit Gaussians agree quite well with the ratio of the means and the statistical standard deviation of the ratios. We therefore conclude that any spatial variation in the RATIO image (i.e. non-uniformity in the UVIS) must be well below the level of statistical fluctuations (5%). The quantitative upper limit on that this places spatial variations in the shield depends on the uncertainty in the width of the Gaussian fit to the distribution of pixel values in the RATIO image, but is probably on the order of 2% or less.

The centroid of the RATIO images can be used to compute the transmission of the shields when combined with the MD data and integration times. We measure the transmission of this shield to be 0.433 at C $K_\alpha$ and 0.411 at O $K_\alpha$.

In the second, more sensitive, analysis method, wavelet decomposition was used to search for non-uniformity at all spatial scales in the RATIO images[1,2]. Two similar programs

| | Mean (counts) | Variance | Std Dev | $\sqrt{Mean}$ |
|---|---|---|---|---|
| IN image | 513.88 cts | 4237.02 | 65.09 cts | 22.67 cts |
| OUT image | 713.046 cts | 7923.84 | 89.02 cts | 26.70 cts |
| Ratio of means ($\mathrm{Mean}_{IN}/\mathrm{Mean}_{OUT}$) | | | | 0.721 |
| Statistical std dev of ratio | | | | **0.042** |
| Gaussian mean of RATIO image | | | | 0.715 |
| Gaussian sigma of RATIO image | | | | **0.043** |
| Transmission at O $K_\alpha$ | | | | **0.411** |

Table 3: Transmission of UVIS S/N 009 at O $K_\alpha$.

were provided by Alexey Vikhlinin for this analysis, and a brief description of the wavelet decomposition technique is given in the Appendix. We assume that all the small scale structure is related to the detector (e.g. hot spots). We use the wavelet decomposition software to find all small scale structures, subtract them from the raw data, and determine what remains.

The wavelet decomposition software did find some structure at both the small (1, 2, and 4 pixel) and intermediate (8, 16, and 32 pixel) scales. Except for a few known hot spots, however, this structure was at a low level, typically less than 1 percent of the average value across the shield. This low level structure is subtracted from the RATIO image, then smoothed with a large Gaussian, showing residual large scale non-uniformity. Contour plots of this residual structure divided by the Gaussian mean determined above are contained in Figures 3 and 4 for the C $K_\alpha$ and O $K_\alpha$ shadowgraphs, respectively. Note that the structure of these two contour plots are quite different, and the level of variation across either is $\sim$1%. The level of significance of these small variations is difficult to assess without further analysis (i.e. Monte Carlo simulations), but it is quite reasonable to conclude that there are no statistically significant large scale non-uniformities at the 2-3% level, in good agreement with the above result.

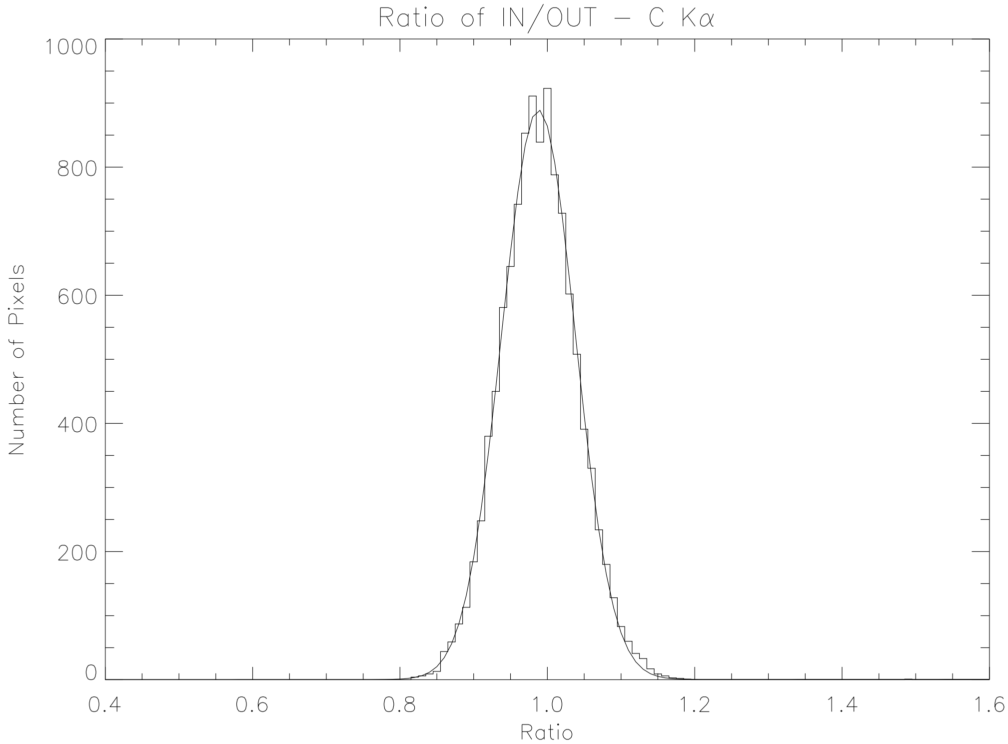


Figure 1: Distribution of pixels in C $K_\alpha$ RATIO image (histogram) and best fit Gaussian (smooth curve).

## 2 Transmission Measurements

We have also made X-ray transmission (in/out) measurements of this UVIS using an LETG facet and a slit (the so-called poor man's monochromator). The facet was inserted in the beam between the UVIS and the X-ray source, and the spectrum dispersed across the MCP. Paddles were inserted to block all direct flux around the grating assembly, and the MD was again used to monitor the temporal stability of the beam. The grating was misaligned by $\sim$1/4 of a degree relative to the detector. This misalignment is considered negligibly small, and was not considered in the analysis described below. Five anodes were used (B, C, Ti, $Mg(OH)_2$, and Cr) providing 7 different energies (B $K_\alpha$, C $K_\alpha$, Ti $L_\iota$, Ti $L_\alpha$, O $K_\alpha$, Cr $L_\iota$,$L_\alpha$ blend, and Mg $K_\alpha$). The dispersive energy resolution of this setup was not high

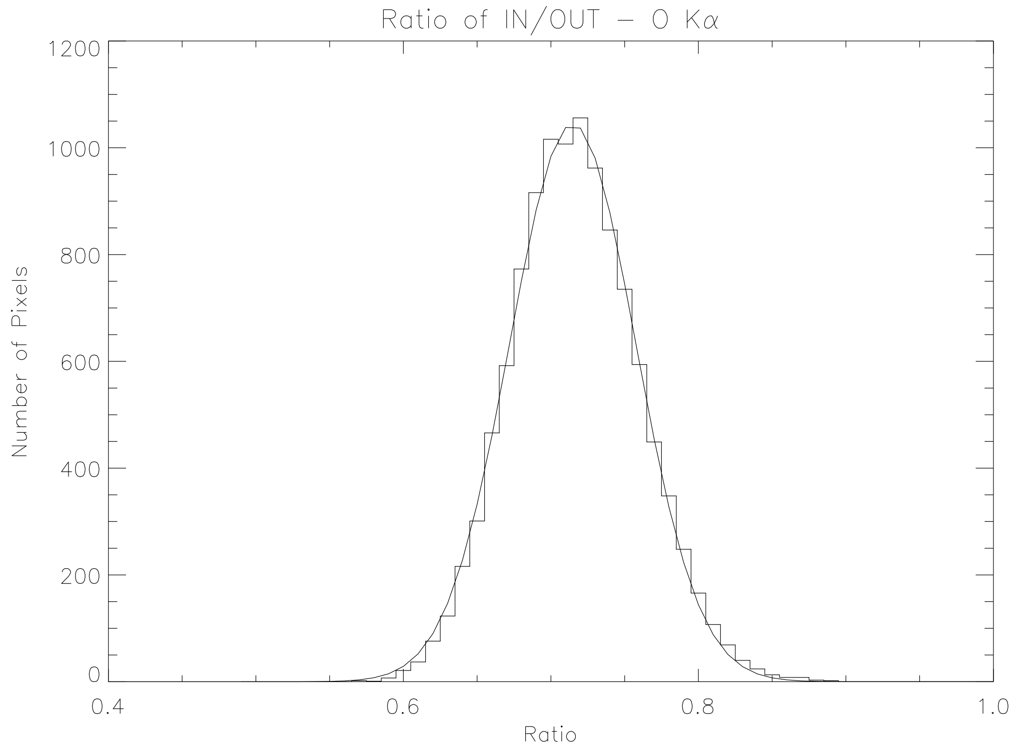


Figure 2: Distribution of pixels in O $K_\alpha$ RATIO image (histogram) and best fit Gaussian (smooth curve).

enough to resolve the Cr $L_\iota$ and $L_\alpha$ lines, so it was assumed that all the flux was at the $L_\alpha$ line. A summary of the measurements at the seven energies is given in Tables 4 and 5.

The raw data were converted to projections at full resolution, and these projections were used to determine the rate in the spectral lines. The line rates (and therefore transmissions) were determined by taking a region of interested around a given spectral line. We only considered a region of the detector that contained the dispersed spectrum to reduce background, and have assumed that higher order contamination is negligible compared to the line flux in first order. Transmission values and uncertainties are listed in Tables 4 and 5. The quoted errorbars are statistical only. Note that the transmission values for the *left* and *right* orders at each energy typically agree within the errorbars, but there is some asymmetry in the flux that is not constant with energy.

| Energy | 183 eV | 277 eV | 395 eV | 452 eV |
|---|---|---|---|---|
| Anode | B on Mg | Graphite | Ti | Ti |
| IN prefix | P1971009j | P1971009b | P1971009g | P1971009g |
| Rate (left order) | 4.50 cts/s | 27.65 cts/s | 2.71 cts/s | 4.17 cts/s |
| Rate (right order) | 4.97 cts/s | 30.42 cts/s | 2.70 cts/s | 4.65 cts/s |
| OUT prefix | P1971009i | P1971009a | P1971009h | P1971009h |
| Rate (left order) | 25.40 cts/s | 62.25 cts/s | 11.26 cts/s | 12.57 cts/s |
| Rate (right order) | 27.86 cts/s | 68.07 cts/s | 11.04 cts/s | 14.09 cts/s |
| **Trans** (left order) | 0.177±0.002 | 0.444±0.003 | 0.241±0.005 | 0.332±0.006 |
| **Trans** (right order) | 0.178±0.002 | 0.447±0.003 | 0.243±0.005 | 0.330±0.006 |
| Shadowgraph trans | | 0.433 | | |

Table 4: Summary of transmission measurements at 4 lower energies.

| Energy | 524 eV | 571 eV | 1253 eV |
|---|---|---|---|
| Anode | $Mg(OH)_2$ | Cr | $Mg(OH)_2$ |
| IN prefix | P1971009c | P1971009f | P1971009c |
| Rate (left order) | 40.54 cts/s | 30.25 cts/s | 121.65 cts/s |
| Rate (right order) | 40.16 cts/s | 29.65 cts/s | 122.53 cts/s |
| OUT prefix | P1971009d | P1971009e | P1971009d |
| Rate (left order) | 96.56 cts/s | 73.37 cts/s | 134.86 cts/s |
| Rate (right order) | 95.67 cts/s | 71.66 cts/s | 135.44 cts/s |
| **Trans** (left order) | 0.420±0.002 | 0.412±0.003 | 0.902±0.004 |
| **Trans** (right order) | 0.420±0.002 | 0.414±0.003 | 0.905±0.004 |
| Shadowgraph trans | 0.411 | | |

Table 5: Summary of transmission measurement at 3 higher energies.

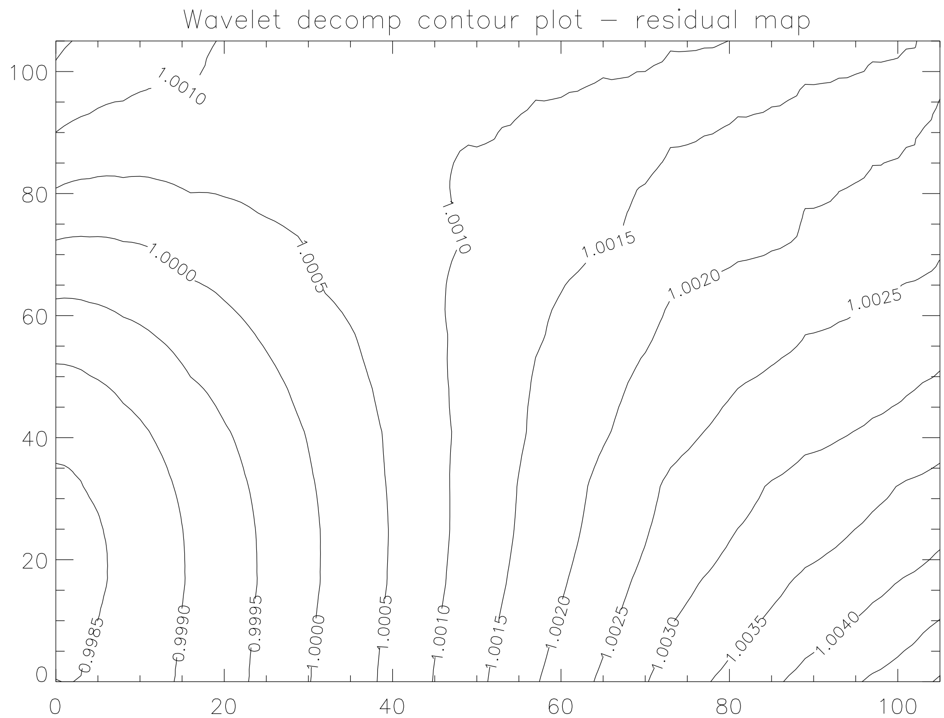


Figure 3: Contour plot of large scale residual non-uniformity of UVIS at C $K_\alpha$

We have fit our standard UVIS absorption model[4] to these transmission data. In this model, we assume that the transmission of the shield can be accurately described by slab absorption of its four main elemental constituents: C, N, O, and Al. The 1982 Henke mass absorption coefficients were used[3]. The free parameters of this model are the areal densities of each of these four elements. The data and best fit model (for *left* and *right* orders) are shown in Figures 5 and 6. The best fit values of the parameters and uncertainties are contained in Table 6. The best fit parameters for the *left* and *right* orders agree with each other within the errorbars in all cases. The reduced chi-square is large for both fits, indicating that our standard UVIS model is a poor description of this data.

For comparison, we have also included in Table 6 parameters of the best fit model of transmission measurements on witness sample TF101-1137 (a witness sample for this shield)

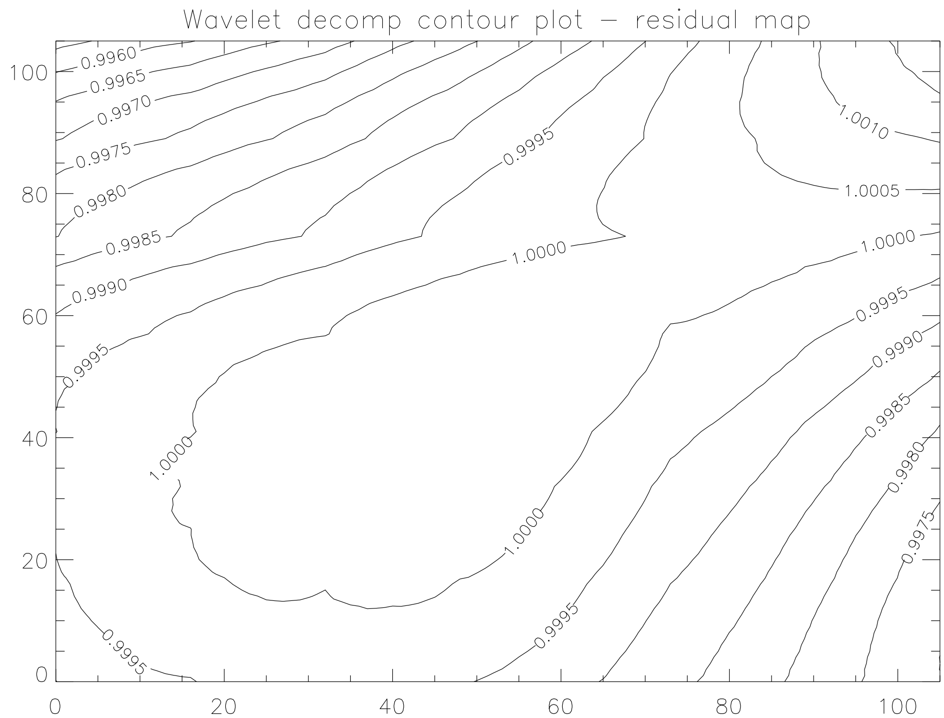


Figure 4: Contour plot of large scale residual non-uniformity of UVIS at O $K_\alpha$

made by Gary M. using the McPherson monochromator. The transmission data for both the *left* order on the shield and the witness sample is contained in Table 7 for reference. The derived Al areal density is the same (within the errorbar) for both the actual shield measurements and the witness sample measurements, but the best fit areal densities of C, N, and O are considerably different. For easy comparison, the *left* transmission and the witness sample measurements, as well as the best fit witness sample model, are plotted together in Figure 7. There clearly are significant differences between the two measurement techniques. Either one (or perhaps both) of the data sets has some significant systematic uncertainty, or the shield and its witness samples have different chemical compositions. While the latter is possible, I view it as improbable without additional supporting evidence, and suspect that there is some systematic error with one of the techniques.

One possible explanation for this discrepancy is higher order contamination in the poorman's monochromator measurements. The differences between the two measurement techniques are largest at the Ti and Cr points, whereas the measured transmissions at C $K_\alpha$ and O $K_\alpha$ are almost identical (and agree well with the transmission determined from the shadowgraph data above). The lines rates from the Ti and Cr anodes are relatively low and the continuum rates are relatively high compared to the graphite and $Mg(OH)_2$ anodes. The high transmission values at the Ti and Cr points will strongly bias the relative abundances of C, N, and O. This will be investigated in more detail for the upcoming HRC-S UVIS measurements. The projections contain the entire dispersed spectra, both lines and continuum, and can be used to estimate higher order contamination with no assumptions about incident flux or detector quantum efficiency.

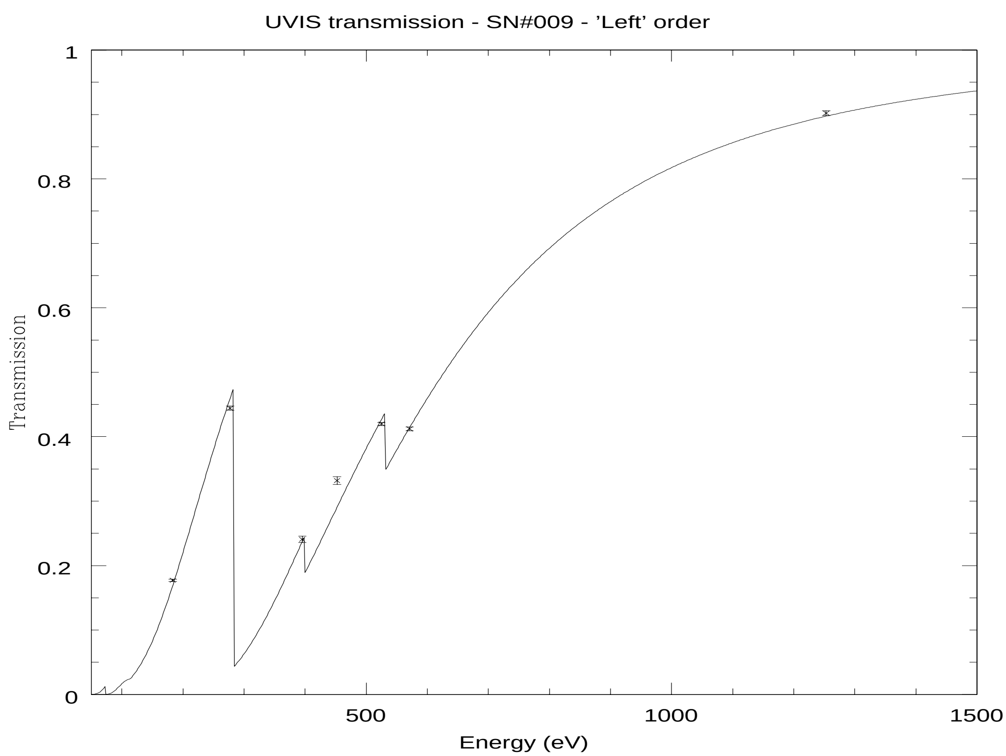


Figure 5: Transmission of HRC-I UVIS S/N 009 - *left* order (points) and best fit model (smooth curve).

| | *left* order | *right* order | TF101-1137 |
|---|---|---|---|
| $\chi^2$ | 75.76 | 76.29 | 14.32 |
| $\chi^2_\nu$ | 25.25 | 25.43 | 2.07 |
| Al areal density | 18.57±0.47 | 18.49±0.46 | 18.16±0.92 |
| C areal density | 45.23±2.51 | 44.98±2.54 | 53.46±1.92 |
| N areal density | 8.82±2.03 | 8.99±2.04 | 5.24±1.67 |
| O areal density | 10.91±1.24 | 10.69±1.24 | 15.37±2.63 |

Table 6: Best fit values and uncertainties of areal density parameters ($\mu$gm/cm$^2$) for *left* and *right* orders, and McPherson monochromator measurements of witness sample TF101-1137.

| Energy (eV) | WS Trans | UVIS Trans (*left*) |
|---|---|---|
| 151.1 | 0.076±0.002 | |
| 183. | | 0.177±0.002 |
| 277.0 | 0.456±0.005 | 0.444±0.003 |
| 395.3 | 0.196±0.003 | 0.241±0.005 |
| 446.7 | 0.267±0.004 | |
| 452.2 | 0.276±0.004 | 0.332±0.006 |
| 511.3 | 0.381±0.005 | |
| 524.9 | 0.404±0.004 | 0.420±0.002 |
| 571 | | 0.412±0.003 |
| 811.1 | 0.677±0.008 | |
| 929.7 | 0.760±0.005 | |
| 1253.6 | 0.872±0.009 | 0.905±0.004 |
| 1486.7 | 0.903±0.014 | |

Table 7: Transmission of UVIS witness sample TF101-1137 measured in the McPherson monochromator and *left* order of UVIS measured with poor-man's monochromator.

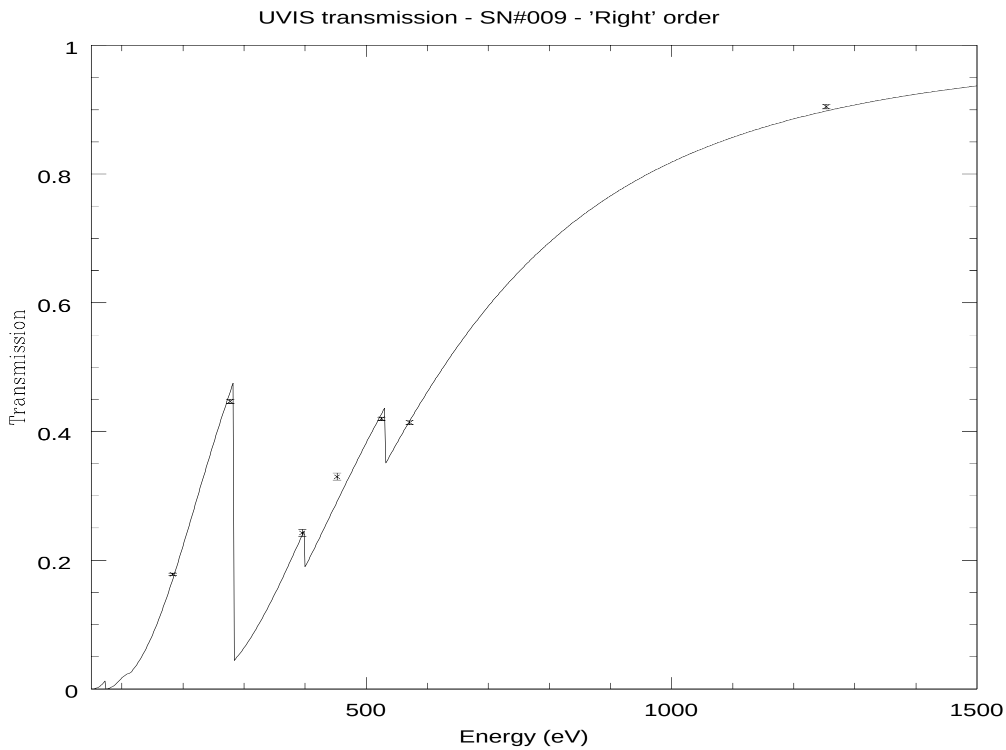


Figure 6: Transmission of HRC-I UVIS S/N 009 - *right* order (points) and best fit model (smooth curve).

# 3 Summary and Conclusion

We have made shadowgraph and X-ray transmission measurements of the flight backup HRC-I UVIS (S/N 009). Analysis of the shadowgraph data using statistical arguments and wavelet decomposition indicate no largescale non-uniformities in the shield greater than ~2%. The results of the X-ray transmission measurements are more difficult to interpret. We have fit our standard UVIS transmission model to the data, and get an unacceptable large value of $\chi^2$. The results also do not agree well with the transmission measurements made on a witness sample of this shield in the McPherson monochromator. In the future, we will investigate the possibility that higher order continuum contamination is biasing these results.

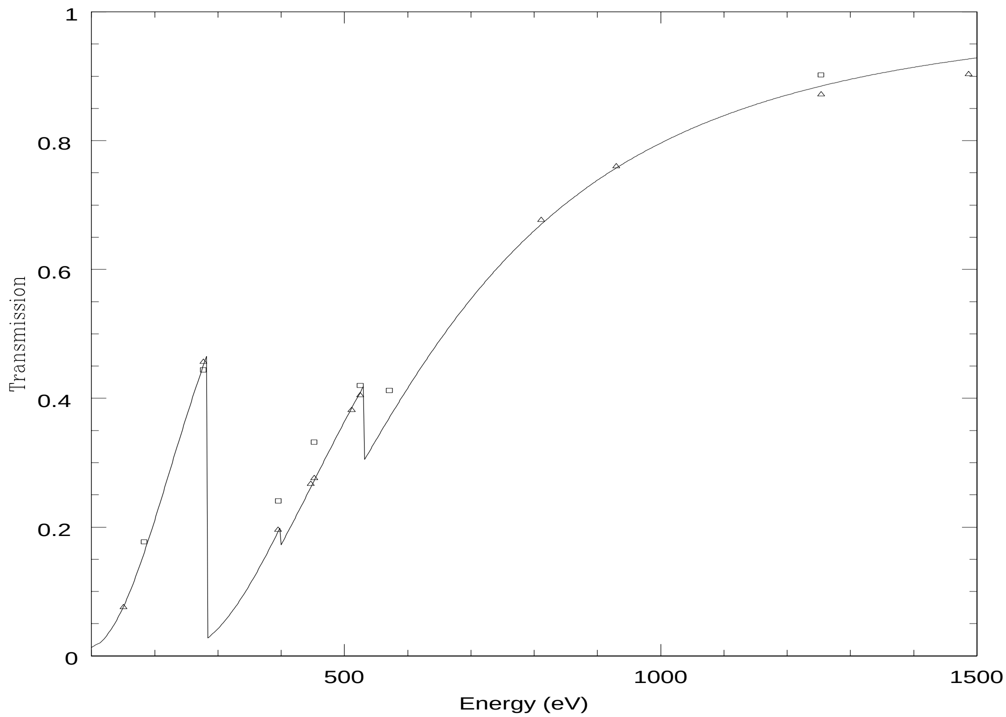


Figure 7: Transmission measurements of *left* order (squares) and witness sample (triangles). The smooth curve is best fit model to the witness sample transmission data. The error bars are approximately the size of the points.

# 4 References


1. A. Vikhlinin, W. Forman, C. Jones, and S. Murray, *Ap. J.*, **451**, 542, 1995.

2. S. A. Grebenev, W. Forman, C. Jones, and S. Murray, *Ap. J.*, **445**, 607, 1995.

3. B. L. Henke, *et al.*, *Atom. Data and Nucl. Data Tables*, **27**, 1, 1982.

4. G. R. Meehan, S. S. Murray. M. V. Zombeck, R. P. Kraft, K. Kobayashi, J. H. Chappell, A. T. Kenter, M. Barbera, A. Collura, and S. Serio, *Proc. SPIE*, ed. O. H. W. Siegmund and M. A. Gummin, **3114**, 1997.

# 5 Appendix: Wavelet Decomposition

The wavelet transform of an image is defined as the correlation of the image with a kernel or analyzing wavelet function. A complete set of kernels is chosen to span all spatial scales of the image, and the transform at a given spatial scale then describes significant structure at that scale. The final result is relatively insensitive to the exact functional form of the kernel. The advantage of the wavelet decomposition over more conventional techniques such as Fourier analysis is that the position, scale, and surface brightness of all features is recovered, and statistical information can be carried through the analysis. A more detailed description of the procedure is given in Grebenev *et al.*[2].

I was provided with two programs to perform this transform by Alexey Vikhlinin. The only differences between the programs is the kernel and the correlation algorithm, and they give similar results. The programs are called wvdecomp and wvdecomp.old. All this software can be obtained from Alexey. The usage of programs is as follows:

wvdecomp input-image output-prefix errimg=errorimage (or stat=gauss) threshold=$T$ thresholdmin=$T_m$

where the *i*nput-image is the name of the input image (FITS format), *o*utput-prefix is the prefix of the output files (FITS format). The *e*rrimg is an optional argument. The file *e*rrorimage (a FITS file) contains the errorbars ($1\sigma$) at every point. If the *i*nput-image is just counts, no optional *e*rrorimage is required. If the *i*nput-image is background subtracted or exposure corrected, the flag *s*tat=gauss may also be appropriate without an *e*rrorimage required. The *t*hreshold sets the detection of significant wavelet components. This number is approximately the Gaussian sigma threshold. The *t*hresholdmin parameter sets the minimum level of significance for a pixel within a structure. At least one pixel in a given structure must be at a significance level above the threshold parameter for that structure to be considered significant. There are several other command line options for this software that are not relevant for this analysis. A more complete description of the command line options is given in /data/alexey/zhtools.pub/HELP.

/RPK